

# Synthesis, Characterization, and Alignment of Magnetic Carbon Nanotubes Tethered with Maghemite Nanoparticles

Il Tae Kim,<sup>†,‡</sup> Grady A. Nunnery,<sup>†</sup> Karl Jacob,<sup>‡</sup> Justin Schwartz,<sup>§</sup> Xiaotao Liu,<sup>§</sup> and Rina Tannenbaum<sup>\*,†,||</sup>

*School of Materials Science and Engineering, Georgia Institute of Technology, Atlanta, Georgia 30332, School of Polymer, Textile, and Fiber Engineering, Georgia Institute of Technology, Atlanta, Georgia 30332, National High Magnetic Field Laboratory, Department of Mechanical Engineering, FAMU-FSU College of Engineering, Florida State University, Tallahassee, Florida 32310, and Department of Chemical Engineering, Technion-Israel Institute of Technology, Haifa 32000, Israel*

Received: December 16, 2009; Revised Manuscript Received: February 15, 2010

In this work we describe a novel, facile method for the decoration of multiwalled carbon nanotubes (MWNTs) with nearly monodisperse  $\gamma\text{-Fe}_2\text{O}_3$  magnetic (maghemite) nanoparticles and their alignment in a magnetic field. The tethering of the nanoparticles was achieved by the initial activation of the surface of the MWNTs with carboxylic acid groups, followed by the attachment of the  $\gamma\text{-Fe}_2\text{O}_3$  nanoparticles via their synthesis using a modified sol–gel process. Sodium dodecylbenzenesulfonate (NaDDBS) was introduced into the suspension as a surfactant in order to prevent the formation of an iron oxide 3D network. Various characterization methods were used to confirm the formation of well-defined maghemite nanoparticles and show that they were tethered to the walls of the MWNTs. The tethered  $\gamma\text{-Fe}_2\text{O}_3$  nanoparticles imparted magnetic characteristics to the MWNTs and allowed their alignment in the direction of an externally applied magnetic field. This facile alignment of MWNTs could promote the enhancement of various properties, e.g., mechanical or electrical properties, of the resulting composites.

## 1. Introduction

Carbon nanotubes (CNTs), discovered by Iijima,<sup>1</sup> are considered among the most promising materials for novel applications, due to their unique mechanical, electrical, thermal, and optical properties.<sup>2–7</sup> Because of their nanoscale dimensions and high surface area, CNTs are also considered as efficient templates for the assembly of nanoparticles,<sup>8</sup> which allow their functionalization with a variety of nanostructures in two and three dimensions. The alignment of CNTs as fillers in various matrices can be used to intensify, reinforce, and enhance some of the properties of the resulting nanocomposites and introduce anisotropy into the material. For example, the alignment of CNTs would be expected to increase the elastic modulus and mechanical strength in the direction of the alignment. Thermal and electrical conductivity would be expected to change in a similar manner. Many groups have achieved CNT alignment by applying electric fields as well as subjecting them to shear flow.<sup>9–13</sup> However, these various attempts have been hampered by the intrinsic tendency of the CNTs to aggregate as a result of their high surface energies.

The decoration of CNTs with various compounds and various structures could increase the tunability of their properties, such as their electrical and magnetic characteristics.<sup>14,15</sup> Recently, various inorganic nanoparticles have been attached to the

external surface of CNTs or filled inside CNTs through several experimental methods.<sup>16,17</sup> In this context, the control of the size of these tethered nanoparticles is of primary importance for the purpose of tailoring the physical and chemical properties of these hierarchical materials.

Iron oxide nanoparticles such as magnetite and maghemite have been of technological and scientific interest due to their unique electric and magnetic properties. These nanoparticles can be used in such diverse fields as high-density information storage and electronic devices.<sup>18–20</sup> Correa-Duarte et al.<sup>21</sup> coated CNTs with iron oxide nanoparticles (magnetite/maghemite) via a layer by layer (LBL) assembly technique and aligned CNT chains in relatively small external magnetic fields. Subsequently, the resulting magnetic CNT structures could be used as building blocks for the fabrication of nanocomposite materials. Cai et al.<sup>22</sup> decorated CNTs with magnetite nanoparticles in liquid polyols. As a result, these nanoparticles could have significant potential for application in the fields of sensors. In addition, Gao et al.<sup>23</sup> initiated the self-assembly of magnetite particles along multiwalled CNTs via a hydrothermal process. The resulting materials feature nanoparticle beads along the CNT surface, rendering this as an appropriate material to be used as a functional device.

Maghemite,  $\gamma\text{-Fe}_2\text{O}_3$ , is the allotropic form of magnetite,  $\text{Fe}_3\text{O}_4$ . These two iron oxides are crystallographically isomorphous. The main difference between the two species is the presence of ferric ions only in  $\gamma\text{-Fe}_2\text{O}_3$ , and both ferrous and ferric ions in  $\text{Fe}_3\text{O}_4$ . As a result, while the magnetic properties of  $\text{Fe}_3\text{O}_4$  are superior,  $\gamma\text{-Fe}_2\text{O}_3$  is more stable, since the iron cannot be further oxidized under ambient conditions. This renders  $\gamma\text{-Fe}_2\text{O}_3$  easier to work with, especially in the presence of organic solvents and organic ligands, and, hence, has been widely used for magnetic storage in a variety of fields such as

\* To whom correspondence should be addressed: phone, (404) 385-1235; fax, (404) 894-9140; e-mail, rinatan@mse.gatech.edu or rinatan@technion.ac.il.

† School of Materials Science and Engineering, Georgia Institute of Technology.

‡ School of Polymer, Textile, and Fiber Engineering, Georgia Institute of Technology.

§ National High Magnetic Field Laboratory, Department of Mechanical Engineering, FAMU-FSU College of Engineering, Florida State University.

|| Department of Chemical Engineering, Technion-Israel Institute of Technology.

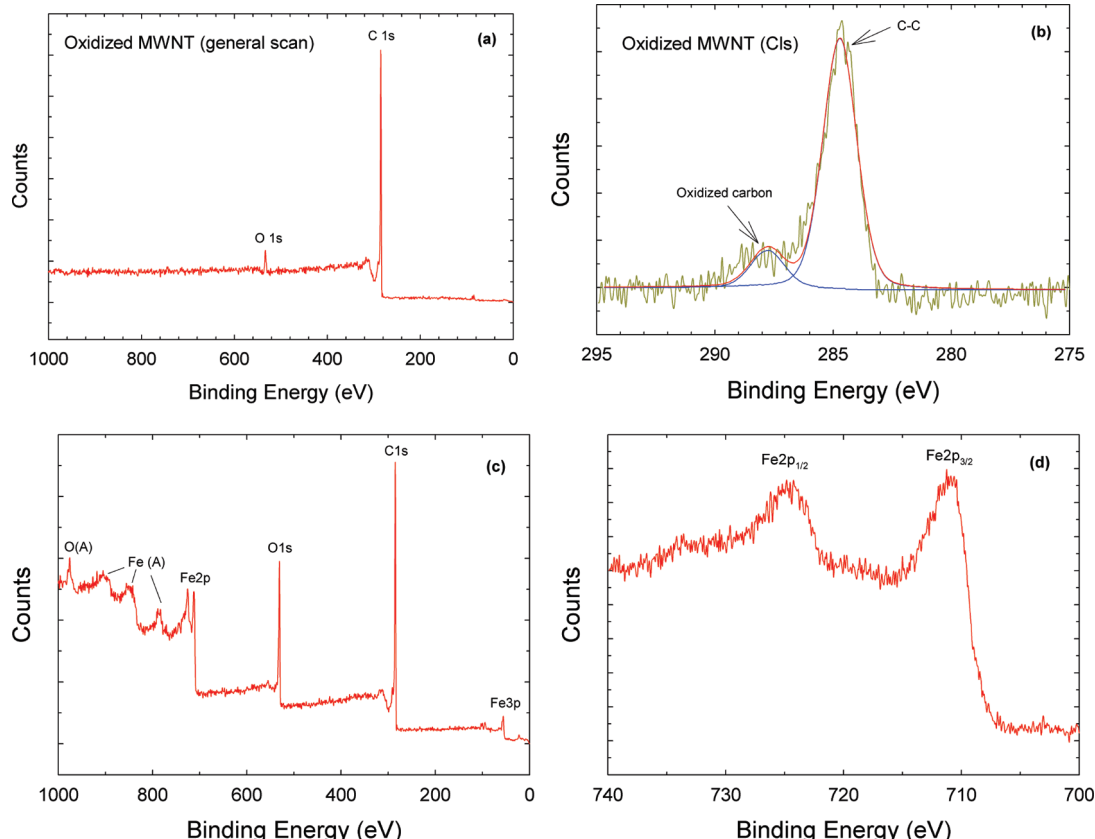
floppy disks and cassette tapes. However, maghemite–CNT nanocomposites have not been studied as extensively as magnetite–CNT nanocomposites, with the exception of several examples. Liu et al.<sup>24</sup> decorated multiwalled CNTs with maghemite via the pyrolysis of ferrocene at different temperatures. This product is expected to provide an efficient way for the large-scale fabrication of magnetic CNT composites. Youn et al.<sup>25</sup> decorated single walled carbon nanotubes (SWNTs) with iron oxide nanoparticles along the nanotube via a magneto-evaporation method. The nanotubes were aligned vertically on ITO surfaces, suggesting the possibility of rendering this process adequate and cost-effective for mass production. The method described in this work consisted of the use of an iron–oleate complex, oleic acid, and truncated SWNTs to create iron oxide nanoparticles. The research also demonstrated the anisotropic properties of vertically aligned SWNTs in a nanocomposite by comparing current densities of the aligned and nonaligned CNTs.

In this paper, we describe and report a convenient approach for the decoration of MWNTs with near-monodisperse maghemite nanoparticles by employing a simple, modified sol–gel process (*in situ* process) with an iron salt as precursor, followed by

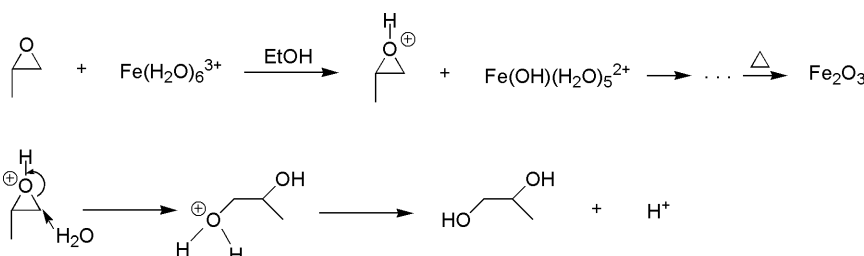
calcination, and focus on the detailed characterization of the product, i.e., the resulting nanocomposite materials, in order to create a sound basis for potential future applications. The locations of the maghemite nanoparticles attachment and their controlled particle size on the surface of the MWNTs are determined not only by different temperatures but also by the mass ratio of the precursor iron salt to the MWNTs. The resulting nanomaterials are superparamagnetic at room temperature and, hence, are conducive to facile alignment under relatively low magnetic field. This general approach could greatly facilitate the formation of highly anisotropic materials that would benefit from the enhancement of properties mediated by CNT alignment in various matrices.

## 2. Experimental Section

**Materials.** This experiment was performed with multiwalled carbon nanotubes (MWNTs) (>99%) produced by chemical vapor deposition followed by HCl mineralization. The diameter of the MWNTs is estimated at 12 nm and the length around 10 nm. For the formation of a surface carboxylate group along the MWNTs, concentrated sulfuric acid (98%) and concentrated

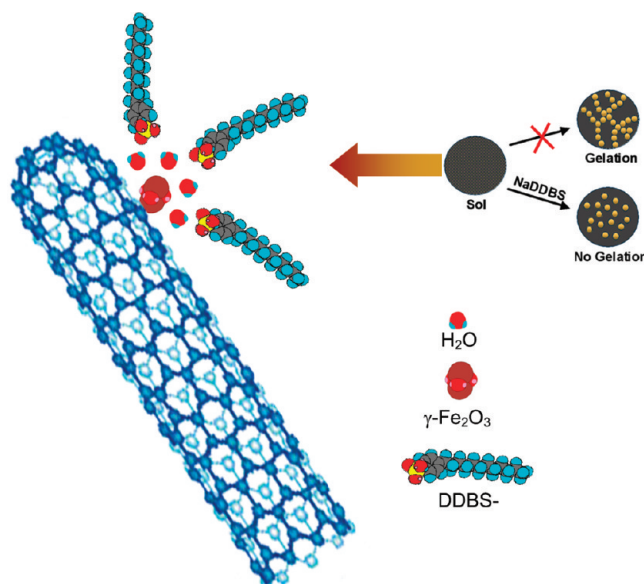


**Figure 1.** (a) The XPS survey spectrum of oxidized and activated MWNTs. (b) The high-resolution XPS spectrum of C 1s, which shows oxidized carbon in the form of a carboxylate group at a binding energy of 288 eV. (c) The XPS survey spectrum of MWNT/ $\gamma$ -Fe<sub>2</sub>O<sub>3</sub>. (d) The high-resolution XPS spectrum of Fe 2p bands.

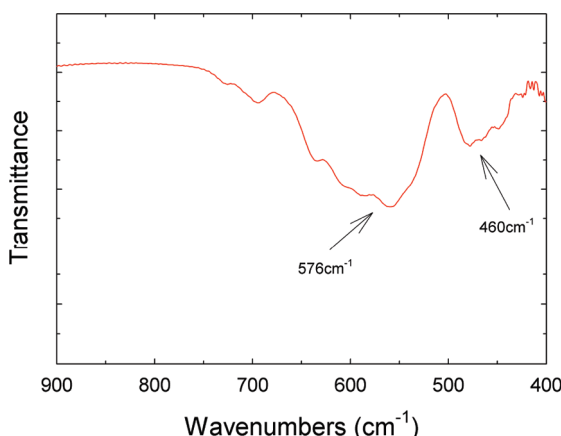


**Figure 2.** The general mechanism of  $\gamma$ -Fe<sub>2</sub>O<sub>3</sub> formation by the addition of propylene oxide to a hydrated iron nitrate solution.<sup>31</sup>

**SCHEME 1:** Hydration Sphere around Iron(III) Centers Coordinated with the NaDDBS Surfactant Molecules<sup>a</sup>



<sup>a</sup> The presence of NaDDBS molecules may be responsible for the inhibition of the formation of the gel.

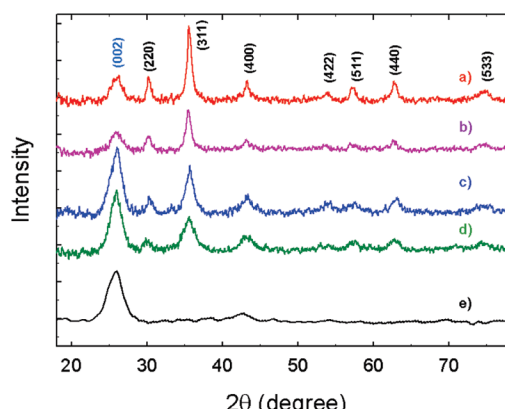


**Figure 3.** FTIR spectrum of MWNT/ $\gamma$ -Fe<sub>2</sub>O<sub>3</sub> after calcinations at 600 °C.

nitric acid (70%) were purchased from Fisher Scientific. And for the preparation of magnetic carbon nanotubes, ferric nitrate nonahydrate, Fe(NO<sub>3</sub>)<sub>3</sub>·9H<sub>2</sub>O was purchased from Acros Organics. Propylene oxide (>99%), C<sub>3</sub>H<sub>6</sub>O (1,2-epoxide), and absolute ethanol (anhydrous, 200 proof) were purchased from Aldrich and used as received. Sodium dodecylbenzenesulfonate (NaDDBS, from TCI) was used in the same concentrations and methods as described in the work of Matarredona et al.<sup>26</sup>

**Carboxylation.** The MWNTs were first dispersed in a solution of concentrated sulfuric acid and concentrated nitric acid (a 3:1 volume ratio). The samples were sonicated in a typical ultrasound bath for 3 h. This acid mixture containing MWNTs was diluted to 25% of its original concentration. Then, the oxidized MWNTs were filtered with a PTFE filter membrane (Alltech, 0.45  $\mu$ m pore size) with the aid of vacuum pump. The MWNTs were washed several times vigorously during filtration in order to reach neutral pH. Then MWNTs were dried in the vacuum oven at 50 °C overnight.

**Synthesis of Maghemite–MWNT Nanostructure.** This work was done by a modified sol–gel process. For the synthesis with Fe(NO<sub>3</sub>)<sub>3</sub>·9H<sub>2</sub>O, 0.65 g of Fe(NO<sub>3</sub>)<sub>3</sub>·9H<sub>2</sub>O was added to 20 mL of absolute ethanol (100% purity) and stirred until



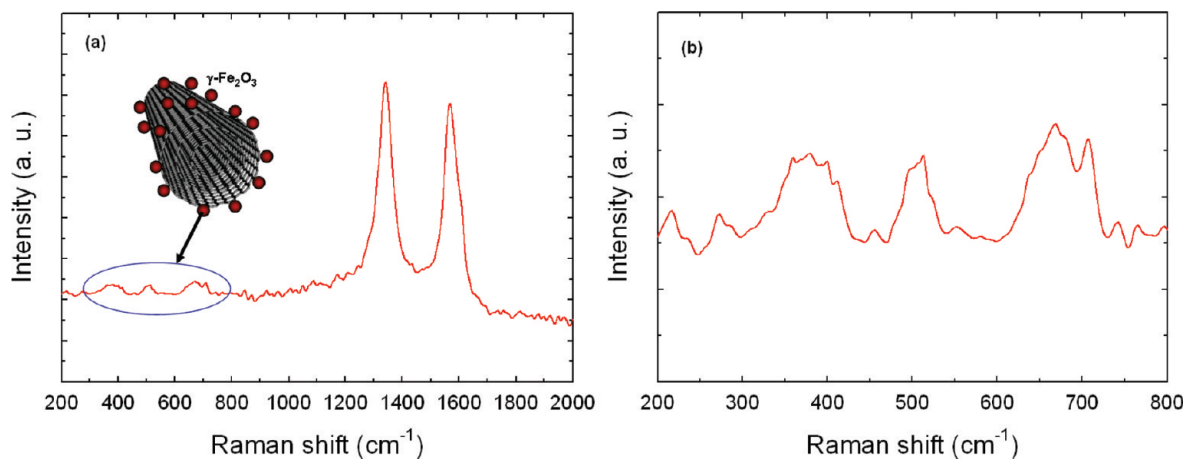
**Figure 4.** The XRD patterns of MWNT/ $\gamma$ -Fe<sub>2</sub>O<sub>3</sub> nanostructures fabricated with two different mass ratios of Fe(NO<sub>3</sub>)<sub>3</sub>·9H<sub>2</sub>O and MWNTs: (a) 4:1 at 600 °C; (b) 4:1 at 500 °C; (c) 2:1 at 600 °C; (d) 2:1 at 500 °C; (e) MWNT.

Fe(NO<sub>3</sub>)<sub>3</sub>·9H<sub>2</sub>O was dissolved completely. This solution was added by oxidized MWNTs, stirred, and sonicated for 3 h. Twenty milliliters of 1.2 mM NaDDBS was added to the solution, the mixture was stirred, and then 1.2 mL of propylene oxide was added as a gelation agent and stirred. The mixture was then placed in a Fisher Scientific isotemperature oven for drying for 72 h at 100 °C. The resulting powder products were washed with water and ethanol several times and dried at 50 °C. The calcinations of these powders were performed at different temperatures in a furnace under nitrogen atmosphere.

**Characterization.** The dried samples were ground into a fine powder using a ceramic mortar and pestle. Tiny amounts of samples were rarified with KBr powder, ground, and pressed in a KBr pellet with a punch and die. A Nicolet Nexus 870 spectrometer scanned the range from 4000 to 400  $\text{cm}^{-1}$  with a resolution of 2  $\text{cm}^{-1}$  and data spacing of 0.964  $\text{cm}^{-1}$ . X-ray photoelectron spectroscopy (XPS) scans of powder samples were taken using a Surface Science Laboratories SSX-100 ESCA spectrometer using monochromatic Al K $\alpha$  radiation (1486.6 eV). X-ray diffraction (XRD) measurement was performed with a X'pert Pro Alpha-1 (wavelength of 1.54 Å). XRD peaks were collected from  $2\theta = 0^\circ$  to  $90^\circ$  with a step size of 0.02°. Raman spectra were recorded in the range of 200–2000  $\text{cm}^{-1}$  at ambient temperature using a WITEC Spectra Pro 2300I spectrometer equipped with an Ar-ion laser, which provided a laser beam of 514 nm wavelength. Transmission electron microscopy (TEM) samples were prepared by placing a droplet of solution onto a TEM grid, and these samples were analyzed using the Hitachi HF2000, 200 kV transmission electron microscope. The alignment of sample was conducted by magnet (GMW-5403) at 0.3 T, and aligned features of samples were characterized using scanning electron microscopy (SEM) (LEO 1530). The samples for SEM were prepared by dispersing as-prepared nanostructures in water solution with surfactant, sonicating for 30 min, and then depositing the samples onto silicon wafer under an external field. The magnetic properties of MWNTs were measured using a 5.5 T Quantum Design superconducting quantum interface device (SQUID) magnetometer at the National High Magnetic Field Laboratory (NHMFL) at the Florida State University.

### 3. Results and Discussion

The most significant and novel result of this report is the decoration of carbon nanotubes with both well-defined and well-dispersed maghemite nanoparticles via a simple, modified sol–gel synthesis and, consequently, their alignment when



**Figure 5.** (a) The Raman spectrum of MWNT/ $\gamma$ -Fe<sub>2</sub>O<sub>3</sub> nanostructure prepared at 600 °C with the mass ratio of 4:1. (b) The detailed Raman spectrum of the same sample in the 200–800 cm<sup>-1</sup> spectral range.

subjected to a magnetic field. The key step for imparting magnetic properties to the carbon nanotubes consists of a carefully designed synthesis method that involves a modified sol–gel process. Other methods to obtain such iron oxide nanoparticles reported to date require high-pressure and hazardous environments such as the generation of hydrogen gas, which can be difficult and costly to produce in bulk.<sup>27,28</sup> However, the modified sol–gel process we present here constitutes a simple and economical process for the formation of iron oxide nanoparticles tethered to carbon nanotubes.

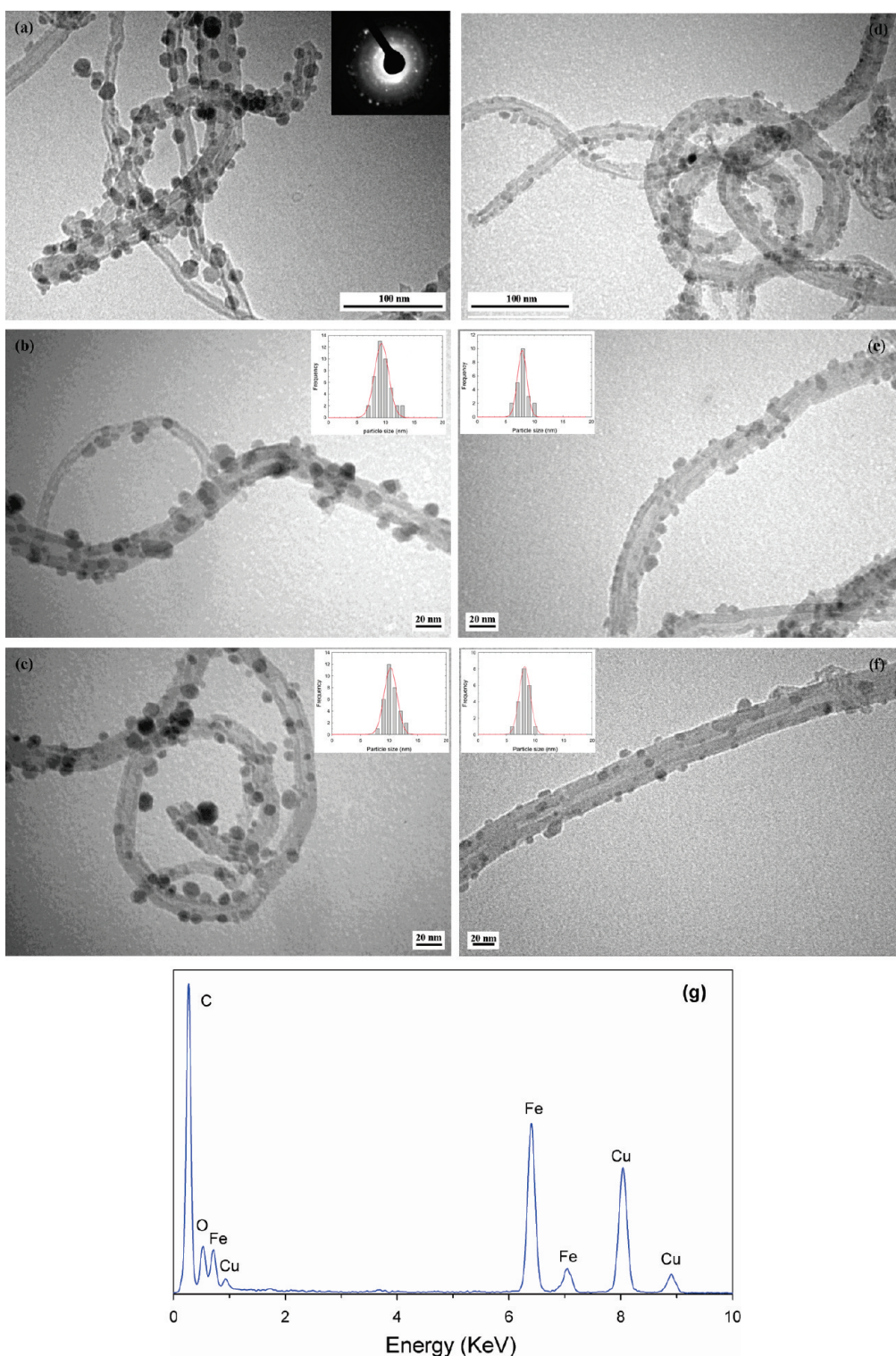
As a first step, the MWNTs were carboxylated in order to introduce negative charges on their surface, which in turn will interact with Fe(III) ions present in a strong acid solution. This process was also coupled with sonication to ensure dispersion of the MWNTs in the suspension. The XPS wide-survey (Figure 1a) and high-resolution spectra (Figure 1b) reveal not only the presence of carbon–carbon bonding of MWNTs at 285 eV binding energy but also the formation of a carbonyl moiety consistent with carboxylated groups at 288 eV binding energy.

The formation of Fe<sub>2</sub>O<sub>3</sub> is dependent upon the presence of propylene oxide, which functions as an oxide promoter. The general mechanism of Fe<sub>2</sub>O<sub>3</sub> formation by the addition of an epoxide to a hydrated iron nitrate solution assumes that propylene oxide behaves as a weak base (Figure 2) that is known to form iron oxide due to the rapid reaction of the base with the metal ion.<sup>29</sup> Effectively, the propylene oxide acts as a “proton scavenger”, since it extracts protons from the water molecules coordinated to the iron salt, resulting in a protonated epoxide. Subsequently, the protonated epoxide undergoes ring-opening by reacting with a nucleophile, such as a nitrate ion or water. As a result of this ring-opening reaction, deprotonation of the hydrated metal complex occurs, and a diol is formed in conjunction with a net decrease of proton concentration in the solution. After further hydrolysis and condensation of the initial hydrated metal complex, increased heating results in the formation of Fe<sub>2</sub>O<sub>3</sub>.<sup>30–32</sup> The gelation occurs as a result of a drying process when metal oxide particles are in the growth stage. If there is no surfactant, metal oxide particles would eventually grow and coalesce, which could form gels. In our system, the occurrence of gelation was inhibited by the addition of a surface active molecule, NaDDBS, which interferes in the growth stage of the iron oxide nanoparticles (gel phase) and prevents the formation of a gel. This occurs because the NaDDBS molecules would have already coordinated to the iron(III) centers (Scheme 1) due to the attraction between the negatively charged hydrophilic head of the surfactant and

the positively charged iron.<sup>26,33</sup> Hence, while it is appropriate to refer to this method as a *modified* sol–gel process, it is important to note that the surfactant inhibits the formation of a gel if introduced into the reaction system at the appropriate stage,<sup>33</sup> i.e., before gelation can occur. In addition to inhibiting gel formation, the NaDDBS molecules also stabilize the nanoparticles (Scheme 1). Because the NaDDBS molecules were added before the addition of the propylene oxide and in the presence of excess water, they have formed a self-assembled protective layer around the iron. This coordination has been able to prevent the approach of the propylene oxide molecules within the coordination sphere of the iron centers, which would have resulted in the formation of a gel. Therefore, due to the presence of the NaDDBS molecules, no aggregates of  $\gamma$ -Fe<sub>2</sub>O<sub>3</sub> were formed but rather the nanoparticles remained individually isolated.

The FTIR spectrum of the product of this modified sol–gel process shows the presence of well-crystallized iron oxide nanoparticles after calcination at 600 °C (Figure 3). Maghemite ( $\gamma$ -Fe<sub>2</sub>O<sub>3</sub>) has an inverse spinel structure, and therefore, it can be seen as an iron-deficient form of magnetite. If the powder is not heat-treated, a weak peak from 800 to 400 cm<sup>-1</sup> is shown. This is evidence of an amorphous iron oxide phase with minimal long-range order typical of maghemite or magnetite. However, after calcination, IR bands show strong peaks at 576 and 460 cm<sup>-1</sup>, which correspond to a partial vacancy ordering in the octahedral positions in the maghemite crystal structure.<sup>34–36</sup>

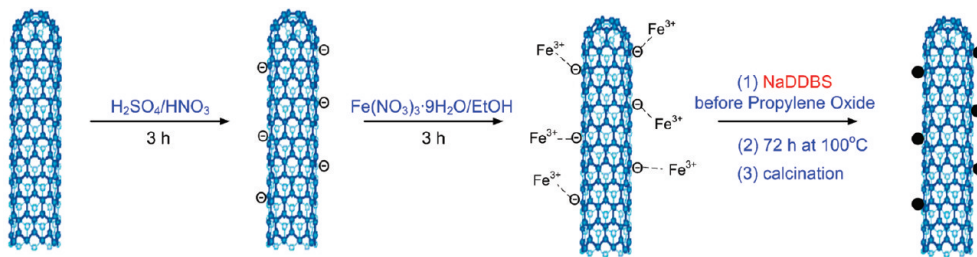
X-ray diffraction patterns of MWNT containing iron oxide nanoparticles calcinated at different temperatures with the initial Fe(NO<sub>3</sub>)<sub>3</sub>·9H<sub>2</sub>O:MWNTs mass ratio of 4:1 and 2:1 demonstrate the high crystalline nature of the nanoparticles (Figure 4). The diffraction peak at  $2\theta = 26^\circ$  can be confidently indexed as the (002) reflection of the MWNTs, similar to that of pure MWNTs. The other peaks in the range of  $20^\circ < 2\theta < 80^\circ$  correspond to the (220), (311), (400), (422), (511), (440), and (533) reflections of maghemite ( $\gamma$ -Fe<sub>2</sub>O<sub>3</sub>) and/or magnetite (Fe<sub>3</sub>O<sub>4</sub>). When the mass ratio of Fe(NO<sub>3</sub>)<sub>3</sub>·9H<sub>2</sub>O and MWNTs increases from 2:1 to 4:1, the intensity of the carbon (002) reflection decreases. Also, when calcination temperature increases from 500 to 600 °C, the crystal structure of the product becomes better-defined. Because XRD patterns of maghemite and magnetite are practically identical,<sup>24</sup> X-ray diffraction alone cannot be used to distinguish between the two phases. Therefore, we employed additional experimental techniques to discern between these two phases.



**Figure 6.** TEM images of maghemite–MWNT prepared with 4:1 mass ratio of  $\text{Fe}(\text{NO}_3)_3 \cdot 9\text{H}_2\text{O}$  and MWNT: (a) low magnification image calcinated at 600 °C (inset: the electron diffraction pattern of the iron oxide nanoparticles); (b) high-resolution (HRTEM) image calcinated at 500 °C; (c) high magnification image calcinated at 600 °C, TEM images of maghemite–MWNT prepared with 2:1 mass ratio of  $\text{Fe}(\text{NO}_3)_3 \cdot 9\text{H}_2\text{O}$  and MWNT; (d) low magnification image calcinated at 600 °C; (e) high magnification image calcinated at 500 °C; (f) high magnification image calcinated at 600 °C; (g) EDS of the maghemite–MWNT composite material.

X-ray photoelectron spectroscopy (XPS) as well as Raman spectroscopy confirmed that the iron oxide nanoparticles formed were indeed maghemite and not magnetite. After the formation of oxidized MWNTs decorated with iron oxide nanoparticles followed by calcination at 600 °C, XPS shows characteristic iron peaks in addition to carbon and oxygen (Figure 1c,d). The position of the Fe (2p<sub>3/2</sub>) and Fe (2p<sub>1/2</sub>) peaks were marked at

711.3 and 724.4 eV, respectively, which are in good agreement with the values reported for  $\gamma\text{-Fe}_2\text{O}_3$  in the literature.<sup>37,38</sup> Therefore, this suggests the formation of  $\gamma\text{-Fe}_2\text{O}_3$  in our samples. Raman spectroscopy can also effectively distinguish between maghemite and magnetite nanoparticles. The strong peak at  $\sim 1350\text{ cm}^{-1}$  can be assigned to the D band of MWNTs, while another dominant peak at  $\sim 1576\text{ cm}^{-1}$  can be ascribed to the G

**SCHEME 2:** Schematic Representation of the Overall Strategy for the Preparation of MWNTs/ $\gamma$ -Fe<sub>2</sub>O<sub>3</sub> Magnetic Carbon Nanotubes via a Modified Sol–Gel Process


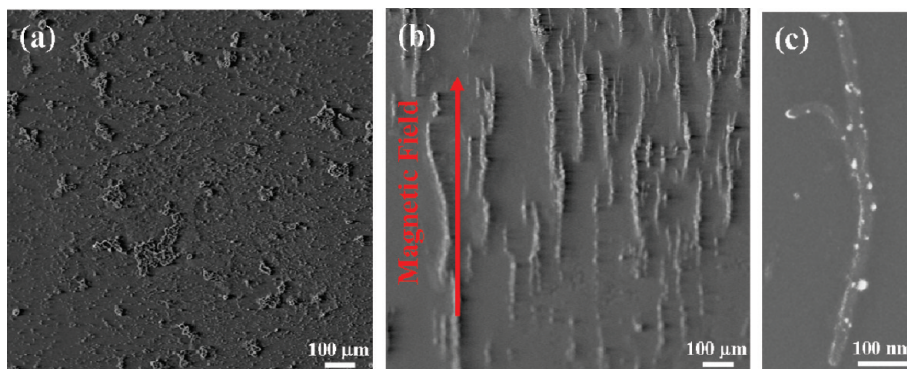
band of MWNTs (Figure 5a).<sup>39</sup> In contrast to magnetite, the maghemite bands are not well-defined but rather consist of several broad peaks around 350, 500, and 700 cm<sup>-1</sup> (Figure 5b),<sup>36</sup> which are unique to these species and are absent in other types of iron oxide nanoparticles. This supports the conclusion that the nanoparticles bound at the walls of the MWNTs are maghemite and not magnetite. When we followed the same experimental method in the absence of carbon nanotubes, the iron oxide nanoparticles that were formed at 600 °C consisted of  $\alpha$ -Fe<sub>2</sub>O<sub>3</sub>, as determined by XRD. Clearly, the presence of the carbon nanotubes affected the structure of the maghemite species obtained, supporting the notion that the nucleation and growth of these particles were intimately driven by their attachment to the surface of the MWNT.

Transmission electron microscopy (TEM) images of MWNTs/ $\gamma$ -Fe<sub>2</sub>O<sub>3</sub> confirmed that  $\gamma$ -Fe<sub>2</sub>O<sub>3</sub> was attached to the walls of the MWNTs. At a mass ratio of 4:1 between the Fe(NO<sub>3</sub>)<sub>3</sub>·9H<sub>2</sub>O precursor and the MWNTs, the particle size increased with increasing temperature from 500 to 600 °C, and the average sizes were 10.1 and 10.8 nm, respectively (Figure 6b,c). Similarly, when the mass ratio of Fe(NO<sub>3</sub>)<sub>3</sub>·9H<sub>2</sub>O precursor and MWNT was 2:1, the average particle sizes as a result of the increased temperature were 7.9 and 8.4 nm, respectively (Figure 6e,f), which also slightly increased with increasing temperature. This result indicated that both a higher mass ratio between the Fe(NO<sub>3</sub>)<sub>3</sub>·9H<sub>2</sub>O precursor and the MWNT and increasing temperature led to larger nanoparticles, and therefore, we can conclude that particle size could be controlled by both the precursor to MWNT mass ratio and temperature. The selected area electron diffraction (SAED) pattern of the sample shows clear diffraction spots (Figure 6a), which indicates the high crystallinity of maghemite. Chemical analysis using EDS during the TEM analysis showed the presence of Fe, O, and C in the maghemite–MWNT system (Figure 6g) and the calculated atomic ratio of Fe and O was close to 2:3, which suggested the formation of  $\gamma$ -Fe<sub>2</sub>O<sub>3</sub>.

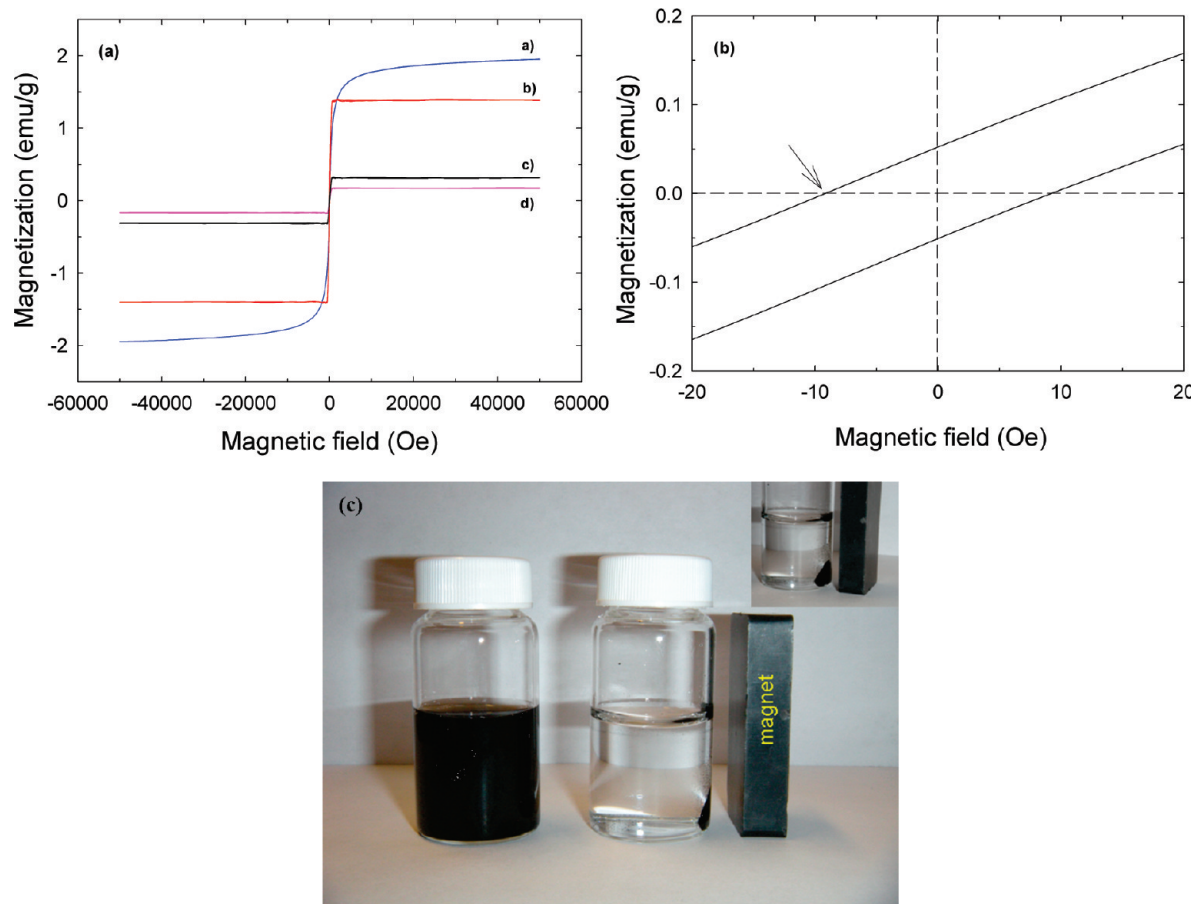
The separation of the nanoparticles on the surface of the MWNT was achieved by electrostatic interactions between the various reactive species in the system. When MWNTs (having negative surface charges as a result of their prior treatment with acid) were added to a Fe(NO<sub>3</sub>)<sub>3</sub>·9H<sub>2</sub>O solution and sufficiently sonicated, electrostatic interactions developed between the surface and the Fe centers due to the positive charges of Fe(III) (Scheme 2). Since the surface sites having negative charges are homogeneously distributed and separated from each other on the surface of the MWNT, the Fe(III) ions also nucleate accordingly to form well-separated nanoparticles.

To facilitate the alignment of pristine MWNTs or MWNTs that have been surface modified with amines or carboxylic groups, it is usually necessary to subject them to strong magnetic or electric fields.<sup>9,40,41</sup> However, in our system, when a droplet of the reacted dispersion was dried under a relatively low magnetic field (0.3 T), the magnetic MWNTs formed with a mass ratio of 4:1 (ratio between the Fe(NO<sub>3</sub>)<sub>3</sub>·9H<sub>2</sub>O precursor and the MWNTs) were oriented in the plane of a silicon substrate at 300 K (Figure 7b,c), a fact which was made possible by overcoming thermal motion and rotation. However, surface activated but undecorated MWNTs did not exhibit alignment features (Figure 7a). Therefore, we conclude that the decoration of the surface of the MWNTs with nanoparticles with good magnetic response, such as  $\gamma$ -Fe<sub>2</sub>O<sub>3</sub>, can facilitate the alignment of the magnetized carbon nanotubes (i.e., having acquired magnetic properties) even under a relatively low magnetic field. Such nanostructures (i.e., having an aspect ratio  $\gg 1$ ) coming in close to proximity to each other but having parallel magnetization direction at their wall surfaces repel each other and are offset.<sup>42–44</sup> However, these magnetic carbon nanotubes have the north and south poles of their dipolar magnet at their top and bottom tips, a fact which leads to the alignment (Figure 7c).

The magnetic properties of the as-prepared MWNTs/ $\gamma$ -Fe<sub>2</sub>O<sub>3</sub> nanocomposites were measured using a SQUID magnetometer.



**Figure 7.** SEM images of the composite material in the presence of a magnetic field of 0.3 T: (a) surface activated but undecorated MWNTs; (b) aligned maghemite–MWNT (4:1 mass ratio) calcinated at 600 °C; (c) a single maghemite–MWNT aligned in the direction of the magnetic field.



**Figure 8.** (a) Magnetization versus applied magnetic field for the magnetic carbon nanotubes prepared at different mass ratios and temperatures: 4:1 mass ratio of  $\text{Fe}(\text{NO}_3)_3 \cdot 9\text{H}_2\text{O}$  and MWNT at (a) 500 °C and (b) 600 °C, and 2:1 mass ratio of  $\text{Fe}(\text{NO}_3)_3 \cdot 9\text{H}_2\text{O}$  and MWNT at (c) 500 °C and (d) 600 °C. (b) The enlarged hysteresis loop of the maghemite–MWNT structures formed from a 4:1 mass ratio of  $\text{Fe}(\text{NO}_3)_3 \cdot 9\text{H}_2\text{O}$  and MWNT that was calcinated at 600 °C. (c) A photograph of magnetic carbon nanotubes suspended in ethanol in the absence (left image) and in the presence (right image) of an externally placed magnet. The inset magnifies the attraction of the magnetic carbon nanotubes to the magnet.

**TABLE 1: Magnetic Properties As a Function of Both Different Mass Ratio of  $\text{Fe}(\text{NO}_3)_3 \cdot 9\text{H}_2\text{O}$  and MWNT and Different Calcination Temperatures**

| magnetic properties                       | calcination temp (°C) | 2:1 <sup>a</sup> | 4:1 <sup>a</sup> |
|---|-----------------------|------------------|------------------|
| $M_s$ (emu g <sup>-1</sup> ) <sup>b</sup> | 500                   | 0.3              | 2.0              |
|   | 600                   | 0.2              | 1.4              |
| $H_c$ (Oe) <sup>c</sup>                   | 500                   | 4.8              | 2.8              |
|   | 600                   | 6.3              | 9.6              |

<sup>a</sup> Mass ratio of  $\text{Fe}(\text{NO}_3)_3 \cdot 9\text{H}_2\text{O}$  and MWNT. <sup>b</sup> Saturation magnetization. <sup>c</sup> Coercivity.

The magnetization hysteresis loops (Figure 8a,b) were measured in fields between  $\pm 50$  kOe at room temperature. The saturation magnetization ( $M_s$ ) of the samples obtained is below 2 emu g<sup>-1</sup>, which is considerably smaller than that of bulk iron ( $M_s = 222$  emu g<sup>-1</sup>) as shown in Table 1. Coercivity is below 10 Oe, which is larger than that of bulk iron ( $H_c = 1$  Oe). The conclusion drawn from the measurement of magnetic properties is that both samples, having different ratios between  $\text{Fe}(\text{NO}_3)_3 \cdot 9\text{H}_2\text{O}$  precursor and MWNT, exhibit superparamagnetic behavior at room temperature. This should be mainly attributed to the small size of  $\gamma\text{-Fe}_2\text{O}_3$  nanoparticles that were formed in the presence of MWNTs.<sup>45</sup> This result is in good accordance with the TEM observation of the small sizes of the maghemite nanoparticles mentioned above.

The magnetic attraction of our sample was also tested by placing a magnet near a vial containing the maghemite–MWNT nanostructures suspended in ethanol (Figure 8c). Our samples

can be easily dispersed in solution and form a stable suspension. When a magnet approaches the vial, magnetic carbon nanotubes are attracted toward the magnet. This phenomenon illustrates that the maghemite nanoparticles that are anchored on the surface of the MWNTs impart to the composite material a magnetic response similar to that observed with magnetite.

According to our expectations, this novel method for the magnetization of carbon nanotubes through the tethering of magnetic iron oxide nanoparticles with controlled size and site distribution opens up a slew of new opportunities for applications in which the alignment of CNTs not only is desired but is actually required. While many groups have studied strategies to align MWNT/ $\text{Fe}_3\text{O}_4$  nanostructures under external magnetic fields due to their strong magnetic properties, very little attention has been devoted to MWNT/ $\gamma\text{-Fe}_2\text{O}_3$  conjugate nanomaterials. We show here that this latter system also exhibits similar interesting properties and can constitute a facile gateway to MWNT alignment processes under tight morphological control and relatively low magnetic fields. Furthermore, we suggest that in the not-so-distant future this maghemite–CNT hybrid material may be used for biomedical applications such as drug delivery or special medical applications such as cancer diagnosis.<sup>46,47</sup>

#### 4. Conclusions

We report here the synthesis of MWNT/ $\gamma\text{-Fe}_2\text{O}_3$  nanostructures via an easy and novel modified sol–gel process. Our study

shows that NaDDBS molecules are intimately involved in inhibiting the formation of an iron oxide gel. As a result, well-defined and well-dispersed maghemite nanoparticles can be obtained. In addition, the particle size of these nanoparticles could be precisely modulated by changing the temperature and the mass ratio of the  $\text{Fe}(\text{NO}_3)_3 \cdot 9\text{H}_2\text{O}$  precursor and MWNTs. Finally, tethered  $\gamma\text{-Fe}_2\text{O}_3$  magnetic nanoparticles on the surface of MWNTs imparted superparamagnetic properties to the composite material. This facilitated the alignment of the decorated MWNTs under externally applied magnetic field, resulting in the formation of an anisotropic material with enhanced mechanical and electrical characteristics. Future work will aim at the characterization of the anisotropic electrical properties by creating thin films of oriented CNTs or embedding them in polymer matrices to form anisotropic nanocomposites.

**Acknowledgment.** Rina Tannenbaum is also with the Department of Chemical Engineering, Technion, Israel, where she was supported by a Marie Curie Grant through the European Union (EU) and by the Israel Science Foundation, Grant No. 650/06. Il Tae Kim and Grady Nunnery were supported by Paper Science and Engineering (PSE) Graduate Fellowships from the Institute of Paper Science and Technology (IPST) at the Georgia Institute of Technology.

**Supporting Information Available:** FTIR spectra of synthesized MWNT/ $\gamma\text{-Fe}_2\text{O}_3$  before calcination, XRD spectra of hematite, and coercivity. This material is available free of charge via the Internet at <http://pubs.acs.org>.

## References and Notes

- (1) Iijima, S. *Nature* **1991**, *354*, 56–58.
- (2) Lourie, O.; Cox, D. M.; Wagner, H. D. *Phys. Rev. Lett.* **1998**, *81*, 1638–1641.
- (3) Treacy, M. M. J.; Ebbesen, T. W.; Gibsoj, J. M. *Nature* **1996**, *381*, 678–680.
- (4) Zhao, Q.; Grogley, M. D.; Wagner, H. D. *Sci. Tech.* **2001**, *61*, 2139–2143.
- (5) Lukic, B.; Seo, J. W.; Bacsa, R. R.; Delpeux, S.; Beguin, F.; Bister, G.; Fonseca, A.; Nagy, A. J. B.; Kis, A.; Jeney, S. *Nano Lett.* **2005**, *5*, 2074–2077.
- (6) Yakobson, B. I.; Smalley, R. E. *Am. Sci.* **1997**, *85*, 324–337.
- (7) Yu, M. F.; Files, B. S.; Arepalli, S.; Ruoff, R. *Phys. Rev. Lett.* **2000**, *84*, 5552–5555.
- (8) Grzelczak, M.; Correa-Duarte, M. A.; Liz-Marzan, L. M. *Small* **2006**, *2*, 1174–1177.
- (9) Camponeschi, E.; Vance, R.; Al-Haik, M.; Garmestani, H.; Tannenbaum, R. *Carbon* **2007**, *45*, 2037–2046.
- (10) Al-Haik, M. S.; Garmestani, H.; Li, D. S.; Hussaini, M. Y.; Sablin, S. S.; Tannenbaum, R.; Dahmen, K. *J. Polym. Sci., Part B* **2004**, *42*, 1586–1600.
- (11) Garmestani, H.; Al-Haik, M. S.; Dahmen, K.; Tannenbaum, R.; Li, D.; Sablin, S. S.; Hussaini, M. Y. *Adv. Mater.* **2003**, *15*, 1918–1921.
- (12) Kimura, T.; Ago, H.; Tobita, M.; Ohshima, S.; Kyotani, M.; Yumura, M. *Adv. Mater.* **2002**, *14*, 1380–1383.
- (13) Camponeschi, E.; Florkowski, B.; Vance, R.; Garrett, G.; Garmestani, H.; Tannenbaum, R. *Langmuir* **2006**, *22*, 1858–1862.
- (14) Kuang, Q.; Li, S. F.; Xie, Z. X.; Lin, S. C.; Zhang, X. H.; Xie, S. Y.; Huang, R. B.; Zheng, L. S. *Carbon* **2006**, *44*, 1166–1172.
- (15) Korneva, G.; Ye, H.; Gogotsi, Y.; Halverson, D.; Friedman, G.; Bradley, J. C.; Kornev, K. G. *Nano Lett.* **2005**, *5*, 879–884.
- (16) Qu, L. T.; Dai, L.; Osawa, E. *J. Am. Chem. Soc.* **2006**, *128*, 5523–5532.
- (17) Han, L.; Wu, W.; Kirk, F. L.; Luo, J.; Maye, M. M.; Kariuki, N. N.; Li, Y. H.; Wang, C.; Zhong, C. *J. Langmuir* **2004**, *20*, 6019–6025.
- (18) Pu, H. T.; Jiang, F. *J. Nanotechnology* **2005**, *16*, 1486–1489.
- (19) Yi, D. K.; Lee, S. S.; Ying, J. Y. *Chem. Mater.* **2006**, *18*, 2459–2461.
- (20) Sun, S. H.; Murray, C. B.; Weller, D.; Folks, L.; Moser, A. *Science* **2000**, *287*, 1989–1992.
- (21) Correa-Duarte, M. A.; Grzelczak, M.; Maceira, V. S.; Giersig, M.; Liz-Marzán, L. M.; Farle, M.; Sieradzki, K.; Diaz, R. *J. Phys. Chem. B* **2005**, *109*, 19060–19063.
- (22) Wan, J.; Cai, W.; Feng, J.; Meng, X.; Liu, E. *J. Mater. Chem.* **2007**, *17*, 1188–1192.
- (23) Jia, B.; Gao, L.; Sun, J. *Carbon* **2007**, *45*, 1476–1481.
- (24) Sun, Z.; Liu, Z.; Wang, Y.; Han, B.; Du, J.; Zhang, J. *J. Mater. Chem.* **2005**, *15*, 4497–4501.
- (25) Youn, S. C.; Jung, D.; Ko, Y. K.; Jin, Y. W.; Kim, J. M.; Jung, H. *J. Am. Chem. Soc.* **2009**, *131*, 742–748.
- (26) Matarredona, O.; Rhoads, H.; Li, Z.; Harwell, J. H.; Balzano, L.; Resasco, D. E. *J. Phys. Chem. B* **2003**, *107*, 13357–13367.
- (27) Khomutov, G. B.; Kislove, V. V.; Gainutdinov, S. P.; Gubin, A. Y.; Obydenov, S. A.; Pavlov, A. N.; Sergeev-Cherenkov, E. S.; Soldatov, A. L.; Tolstikhina, A. S.; Trifonov, A. S. *Surf. Sci.* **2003**, *532*, 287–293.
- (28) Can, M. M.; Ozcan, S.; Firat, T. *Phys. Status Solidi C* **2006**, *3*, 1271.
- (29) Livage, J.; Henry, M.; Sanchez, C. *Prog. Solid State Chem.* **1998**, *18*, 259.
- (30) Gash, A. E.; Satcher, J. H. J.; Simpson, R. L. *Chem. Mater.* **2003**, *15*, 3268–3275.
- (31) Gash, A. E.; Tillotson, T. M.; Satcher, J. H.; Poco, J. F.; Hrubesh, L. W.; Simpson, R. L. *Chem. Mater.* **2001**, *13*, 999–1007.
- (32) Walker, J. D.; Tannenbaum, R. *Chem. Mater.* **2006**, *18*, 4793–4801.
- (33) Camponeschi, E.; Walker, J. D.; Garmestani, H.; Tannenbaum, R. *J. Non-Cryst. Solids* **2008**, *354*, 4063–4069.
- (34) Millan, A.; Palacio, F.; Falqui, A.; Snoeck, E.; Serin, V.; Bhattacharjee, A.; Ksenofontov, V.; Gütlich, P.; Gilbert, I. *Acta Mater.* **2007**, *55*, 2201–2209.
- (35) White, W. B.; Deangelis, B. A. *Spectrochim. Acta, Part A* **1967**, *23A*, 985.
- (36) deFaria, D. L. A.; Silva, S. V.; deOliveria, M. T. *J. Raman Spectrosc.* **1997**, *28*, 873–878.
- (37) Hyeon, T.; Lee, S.; Park, J.; Chung, Y.; Na, H. *J. Am. Chem. Soc.* **2001**, *123*, 12798–12801.
- (38) Sun, Z.; Yuan, H.; Liu, Z.; Han, B.; Zhang, X. A. *Adv. Mater.* **2005**, *17*, 2993–2997.
- (39) Jorio, A.; Pimenta, M. A.; Filho, A. G. S.; Satio, R.; Dresselhaus, G.; Dresselhaus, M. S. *New J. Phys.* **2003**, *5*, 139.
- (40) Zhu, Y.; Ma, C.; Zhang, W.; Zhang, R.; Koratkar, N.; Liang, J. *J. Appl. Phys.* **2009**, *105*, 054319.
- (41) Steinert, B. W.; Dean, D. R. *Polymer* **2009**, *50*, 898–904.
- (42) Rosensweig, R. E., *Ferrohydrodynamics*, 2nd ed.; Dover: Mineola, NY, 1985.
- (43) Larson, R. G., *The Structure and Rheology of Complex Fluids*; Oxford University Press: New York, 1999.
- (44) Fermigier, M.; Gast, A. P. *J. Colloid Interface Sci.* **1992**, *154*, 522–539.
- (45) Pascal, C.; Pascal, J. L.; Favier, F.; Moubtassim, M. L.; Payen, C. *Chem. Mater.* **1999**, *11*, 141–147.
- (46) Sousa, M. H.; Rubim, J. C.; Sobrinho, P. G.; Tourinho, F. A. *J. Magn. Magn. Mater.* **2001**, *225*, 67–72.
- (47) Sincai, M.; Ganga, D.; Bica, L.; Vekas, J. *J. Magn. Magn. Mater.* **2001**, *225*, 235–240.